HHS Public Access

Author manuscript

ACS Nano. Author manuscript; available in PMC 2016 February 26.

Published in final edited form as:

ACS Nano. 2016 January 26; 10(1): 861–870. doi:10.1021/acsnano.5b05999.

Tumor Presence Induces Global Immune Changes and Enhances Nanoparticle Clearance

Marc P. Kai[†], **Hailey E. Brighton**[‡,§], **Catherine A. Fromen**[†], **Tammy W. Shen**[‖], **J. Christopher Luft**[‖], **Yancey E. Luft**[#], **Amanda W. Keeler**[‖], **Gregory R. Robbins**[‡], **Jenny P. Y. Ting**[‡,⊥], **William C. Zamboni**[‡,‖], **James E. Bear**[*,‡,§,#], and **Joseph M. DeSimone**[*,†,‡,‖,#,▽]

[†]Department of Chemical and Biomolecular Engineering, North Carolina State University, Raleigh, North Carolina 27695, United States

[‡]Lineberger Comprehensive Cancer Center, University of North Carolina at Chapel Hill, Chapel Hill, North Carolina 27599, United States

[§]Department of Cell Biology and Physiology, University of North Carolina at Chapel Hill, Chapel Hill, North Carolina 27599, United States

[‖]School of Pharmacy, University of North Carolina at Chapel Hill, Chapel Hill, North Carolina 27599, United States

[#]Department of Chemistry, Howard Hughes Medical Institute, University of North Carolina at Chapel Hill, Chapel Hill, North Carolina 27599, United States

[⊥]Department of Microbiology-Immunology, University of North Carolina at Chapel Hill, Chapel Hill, North Carolina 27599, United States

[▽]Department of Pharmacology, University of North Carolina at Chapel Hill, Chapel Hill, North Carolina 27599, United States

Abstract

Long-circulating nanoparticles are essential for increasing tumor accumulation to provide therapeutic efficacy. While it is known that tumor presence can alter the immune system, very few studies have explored this impact on nanoparticle circulation. In this report, we demonstrate how the presence of a tumor can change the local and global immune system, which dramatically increases particle clearance. We found that tumor presence significantly increased clearance of PRINT hydrogel nanoparticles from the circulation, resulting in increased accumulation in the liver and spleen, due to an increase in M2-like macrophages. Our findings highlight the need to better understand interactions between immune status and nanoparticle clearance, and suggest that further consideration of immune function is required for success in preclinical and clinical nanoparticle studies.

Graphical abstract

[*]Corresponding Authors: desimone@unc.edu. jbear@email.unc.edu.

Supporting Information: The Supporting Information is available free of charge on the ACS Publications website at DOI: 10.1021/acsnano.5b05999.

Notes: The authors declare no competing financial interest.

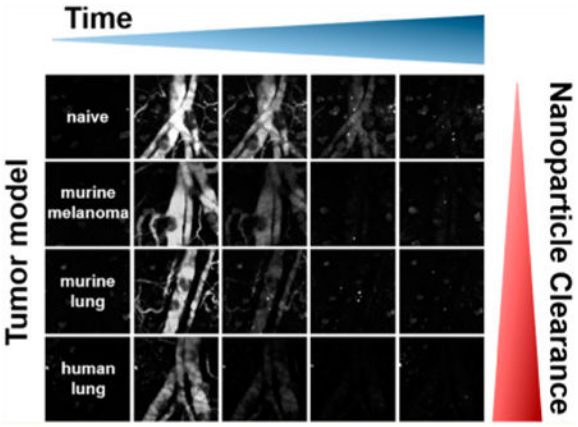

Keywords

nanoparticle; orthotopic; pharmacokinetic; immunology; intravital

Advances at the intersection of material science and biology have led to improved and expanded treatment options in the field of oncology. Research in nanomedicine has resulted in improved therapeutic index, targeting strategies, and biocompatibility of nanoparticle treatments against cancer in the clinic.[1] Major strides in parallel work have also resulted in benefits to the biology component of oncology research, including the development of a human cancer cell line library, which can be used to control variability and identify treatment platforms for preclinical studies.[2] This has led to a variety of selectively optimized particle platforms, which prove successful under narrow preclinical conditions using a particular therapy and model. In clinical settings, however, tumor heterogeneity in patients inhibits the effects of targeted nanotherapies that have proven successful in preclinical models.[3] For example, varying tumor cell growth, incongruous cancer cell genotypes, and different intratumoral immune responses can affect the properties, structure, and content of the tumor microenvironment.[4,5] Certain clinically relevant preclinical models can address and model tumor heterogeneity, such as some patient-derived xenografts and genetically engineered mice (GEM) models, but these systems still exhibit varied responses to different nanoparticle platforms.[6,7] Decades of research have shown that particles must demonstrate certain universal attributes for maximizing circulation persistence, a necessary tenet for passive tumor accumulation.[1] There is, however, an inherent variability among particle characteristics that may depend on the platform or fabrication technology, resulting in a variety of unique optimal combinations of properties for effective therapy.[8] This variability is further complicated by the status of the immune system, which adds a significant layer of complexity.[9]

Regardless of how particle properties are manipulated, the eventual fate of a nanoparticle is typically the liver and spleen, which occurs largely through sequestration by the immune system, specifically by the mononuclear phagocyte system (MPS).[10,11] Interestingly, most studies investigate interactions between nanoparticles and the immune system in either healthy or in immune-compromised mice (*e.g.*, tumor-bearing), but they ignore proper side-by-side comparisons in these models. A better understanding of nanoparticle-immune

system interactions in healthy *versus* immune-compromised mice is necessary, as tumor burden has been shown to cause both local and systemic polarization of the normal balance in the immune system, depending on the model used.[12] In humans, it is well-established that local immune suppression within the tumor microenvironment prevents a natural intervention by the body, mainly through a shift from a Th1 (pro-inflammatory) to a Th2 (anti-inflammatory) or Treg (regulatory) response (reviewed extensively by ref 13). Additionally, a multitude of studies in both humans and animals have shown enhanced myelopoiesis in the marrow and spleen in response to tumor-burden, resulting in a system-wide shift and increased populations of granulocytes and monocytes.[14–16] The bone marrow-derived myelomonocytic cells that reach the tumor often differentiate into tumor-associated macrophages, which are polarized toward a M2-like phenotype (Th2-biased).[17] Recently, Th2 bias in healthy mice was shown to enhance nanoparticle clearance. A study by Jones *et al*. uncovered preferential particle uptake in Th2-prone murine strains.[18] Monocytes, granulocytes, and macrophages in the blood and spleen were responsible for the difference in nanoparticle clearance. However, the final gap between the effect of tumor presence on the immune system and nanoparticle behavior has yet to be bridged.

Ultimately, anecdotal evidence is not sufficient to predict the behavior of a given nanoparticle in a biological setting. Consequently, to increase the chance of successful translation, preclinical efforts should seek to understand particle behavior in the most relevant preclinical animal models available in addition to performing traditional efficacy and toxicity assays. The aim of this study was to investigate the effect of tumor-presence on the behavior of nanoparticles in several orthotopic allograft and xenograft models of cancer, and evaluate the influence of the tumor on immune status and resultant particle clearance. With the use of the Particle Replication in Nonwetting Templates (PRINT) platform, particle parameters were independently and systematically controlled to determine precisely how the immune system affects nanoparticle behavior.[19,20] The modulus, shape, and surface chemistry of PRINT hydrogels were previously optimized to achieve long-circulation.[21,22] Herein, we report the effects of tumor presence on the *in vivo* behavior of PEGylated PRINT hydrogel nanoparticles.

Results

Tumor Burden Induces Pharmacokinetic Modulation

Intravital microscopy (IVM) was used to investigate the circulation profile of nanoparticles in several tumor models.[23,24]

A far-red fluorescent dye was polymerized into PRINT particles to facilitate imaging, and the mouse ear was chosen since the proximity of blood vessels to the surface minimizes the effects of tissue autofluorescence and attenuation. To ensure a valid comparison between different animals, all particles used in these studies were from the same batch, the same dose was injected in each animal, and the instrument settings were kept constant. Three tumor models were investigated and compared to naïve mice. Orthotopic locations were used to mimic clinical conditions for tumor growth and microenvironment. A human lung xenograft (A549) and mouse lung allograft (344SQ) were selected as examples of non-small cell lung cancer (NSCLC), a typical nanomedicine target. A mouse melanoma (LKB498) allograft in

the ear was included to address any effects caused by disrupting the physiology of the lung, an organ with prominent immune function.[25]

Time-lapse imaging of particle fluorescence in the vasculature of the mouse ear postinjection of nanoparticles, shown in Figure 1A, indicated decreased circulation persistence in tumor-bearing mice compared to naïve mice. Quantification of the fluorescence is illustrated in Figure 1B, represented as normalized fluorescence as a function of time. The initial fluorescence for nanoparticles injected in tumor-bearing animals was lower compared to the naïve mice, despite equivalent dosing. Additionally, the initial fluorescence level decreased as a function of tumor model; 344SQ lung was lower than LKB498 ear, and A549 lung was markedly lower than both 344SQ lung and LKB498 ear. Analysis of the fluorescence curves also revealed significantly lower particle exposure in the blood, represented by the area-under-the-curve (AUC), in the presence of a tumor (Figure 1B, inset). Similar to the initial fluorescence trend, the A549 lung had the lowest AUC of the three tumor models investigated.

Upon discovering that circulation of PRINT hydrogels is reduced in tumor-bearing mice compared to naïve controls, longer time points were investigated in order to determine the fate of the nanoparticles in the A549 and 344SQ lung tumor models. To analyze pharmacokinetic (PK) behavior at longer time points, inductively coupled plasma mass spectroscopy (ICP-MS) was employed as an analytical technique.[26] Platinum was incorporated into the particles *via* cisplatin drug complexation and used to track particles in the blood, spleen, and liver. Limited release of the drug from the particle in plasma was validated in previous studies, ensuring platinum detection correlated directly to particle concentration.[27] The circulation profile was examined to extended time points (0.083, 0.5, 1, 6, and 24 h) using ICP-MS. Using this method, we observed the same trend as in the IVM study, as both tumor-bearing models demonstrated faster particle clearance compared to naïve mice (Figure 2A). The A549 lung model also exhibited an initial concentration 2.8-times lower than that for the other particle arms, again despite initial equivalent dosing. This confirmed the phenomenon observed in the IVM fluorescence experiments. Additionally, the circulation behavior of free cisplatin was not altered by the presence of a tumor. This indicated that the mechanism responsible for the difference in clearance was size-dependent. Specific parameters of PK behavior were also evaluated (Figure 2B). As previously discussed, the AUC represents particle exposure or presence in the blood, which correlates to the amount of an entity reaching circulation. The rate of removal of an entity is measured as clearance (CL). The volume of distribution (V_d) is a theoretical value representing the propensity for an entity to stay in the blood compartment (low V_d) compared to being tissue-bound and widely distributed (high V_d). Examination of these PK parameters confirmed the results from the fluorescence experiments. A lower AUC of particles in tumor-bearing mice indicated decreased exposure compared to naïve mice. Increases in CL and V_d for particles in mice with tumors further pointed to more efficient removal of particles from circulation. For all three parameters, particles had favorable values compared to free drug. Figure 2C illustrates the absence of a tumor-based effect on free drug PK parameters.

The primary organs responsible for removing particles from circulation are the liver and spleen. Consequently, these organs were also analyzed for platinum content *via* ICP-MS to

evaluate the fate of the PRINT hydrogel nanoparticles in mice with and without lung tumors (Figure 2D,E). An increase in platinum was observed at early time points in tumor-bearing mice, corresponding with higher particle concentrations. The increased activity by these organs with salient immune cell activity inversely correlated to the plasma circulation profiles; the presence of a tumor decreased plasma circulation and increased sequestration in the liver and spleen compared to naïve mice. Additionally, a large portion of particles were isolated within the first 5 min after injection in the A549 lung mice, indicated by the higher initial level in both the liver and spleen. As observed in plasma, the effect of a tumor on the disposition of free cisplatin was also negligible.

These surprising results suggest that tumor presence dramatically impacts nanoparticle circulation, possibly due to differences in immune status among the groups. The lung has prominent immune function, and if its function is disrupted (*e.g.*, surgery, tumor burden), this could provoke an unintended immune response.[28] We validated that the shift in clearance was not caused by the surgical procedure for tumor inoculation, as tumor-bearing and sham mice experienced the same exact surgical procedure. Tumor-bearing mice received an injection of PBS and Matrigel with A549 cells into the lung as described in Methods, while sham mice received PBS and Matrigel without A549 cells. Naïve mice did not have any surgical procedure or lung injection. No significant difference in circulation was observed between the sham and naïve mice (Supporting Information Figure 1), confirming that the shift in particle circulation was caused by the presence of cancer cells and not by the surgery.

Serum from Tumor-Bearing Mice Increases Macrophage Activity *ex Vivo*

Increased particle clearance within tumor-bearing animals compared to naïve animals of the same strain suggested that tumor presence might influence immune cell function even in regions distal to the tumor. This prompted us to investigate the presence of circulating secretory factors within the serum of tumor-bearing animals that may enhance immune function and particle clearance. To interrogate this *ex vivo*, we harvested bone marrow-derived macrophages and tested their activity in response to control and serum-spiked media, with serum collected from naïve mice and mice bearing A549 lung, 344SQ lung, or LKB498 ear tumors. After incubating macrophages with serum-spiked media for 24 h, we exchanged this media for fresh, nonspiked media, and fluorescent particles were dosed onto the cells. Macrophage activity, demonstrated by fluorescent particle uptake, was significantly enhanced after incubation in serum-spiked media from tumor-bearing mice (Figure 3). The median fluorescent intensity (MFI) of each macrophage, indicating the number of particles internalized, was significantly higher when the cells were incubated with serum collected from tumor-bearing mice compared to naïve mice. Only a slight increase in macrophage activity was observed between macrophages incubated in control media *versus* spiked media containing serum from naïve mice. These *ex vivo* results support the hypothesis that the difference in particle clearance and sequestration by the liver and spleen is, at least in part, caused by a secreted factor within the serum of tumor-bearing mice.

Tumor Presence Increases Particle Recognition by Immune Cells

A shift in the status of immune cells in cancer has been well documented, though less is known about the effect of such polarization on particle behavior. We used flow cytometry to pinpoint the cell populations responsible for increased uptake in the presence of a tumor. Mice with and without A549 lung tumors were injected with fluorescent PRINT hydrogels, and after 2 h, blood, liver, lung, and spleen were collected and digested into single cell suspensions for analysis. This time point exhibited a balance between a large difference in organ accumulation of particles and a sufficient concentration still in circulation. Depicted in Figure 4, several differences in both the cell association and MFI of particles were observed following the introduction of a tumor. In blood, no significant difference in association was observed among the cell populations; however, an increase in the MFI of particles in monocytes (macrophage precursors) was observed (Figure 4A). Lung populations revealed an increase in macrophage association and MFI of particles, and a significant increase in the MFI of particles in dendritic cells (DCs) (Figure 4B). Analysis of the spleen showed negligible differences in association, but an increase in particle MFI for granulocytes (Figure 4C). Finally, the liver displayed a clear increase in particle association with granulocytes and macrophages, with the same trend in MFI for those two populations (Figure 4D). Similar to the lung, a marked increase in the particle MFI in DCs was observed. Overall, the macrophage population was affected most by the presence of a tumor. This manifested as increased recognition of PRINT hydrogel nanoparticles in tumor-bearing mice, evidenced by consistently higher numbers in both cell association and particles per cell across organs. Finally, there was no significant difference in the macrophage population relative to total immune cells (Supporting Information Figure 2).

This consistent difference in particle recognition by macrophages prompted a more detailed analysis of macrophage subpopulations. Macrophages can be skewed toward a M1 or M2-like phenotype; M1 macrophages are associated with an inflammatory response, such as defense host infection, whereas M2-like macrophages are associated with an anti-inflammatory response, such as tissue repair.[29] M2-like polarization is common in tumor-associated macrophages,[30] and results from this work revealed a difference in subpopulation distribution in mice with A549 tumors. Flow cytometry was used to identify M1 *versus* M2-like phenotypes based on a difference in the expression of CD206, the macrophage mannose receptor (MMR), which is significantly up-regulated in M2-like macrophages.[31] Representative histograms illustrate the difference in CD206 expression on macrophages isolated from mouse livers (Figure 5A). Quantification of this MMR expression revealed a shift in the proportion of macrophage subsets in the spleen and liver of mice with and without A549 lung tumors (Figure 5B). In the spleen, the percentage of macrophages that expressed CD206 increased from 29.6% in naïve mice to 45.8% in tumor-bearing mice. The same trend in MMR expression was observed in liver macrophages, which shifted from 13.7% to 37.1% in naïve and A549 lung mice, respectively. Overall, macrophages in the spleen and liver of tumor-bearing mice were skewed toward a M2-like phenotype. There was no significant difference in populations among the lung macrophages.

When the particle association was measured in these two macrophage populations, differences were observed between the organs of naïve and tumor-bearing mice (Figure 6).

When a tumor was present, particles associated more with M1 macrophages in the lung and liver compared to the naïve mice (Figure 6A,C; top). In the liver, the M2-like population also had higher particle association when a tumor was present. This was consistent with the overall increase in macrophage association seen in Figure 4B,D. The spleen had no significant difference in association for either population. Quantification of the median fluorescence in each organ revealed a higher uptake of fluorescent particles in both macrophage subsets from tumor-bearing *versus* naïve mice. Upon examination of the MFI in M1 macrophages of the lung and liver, there was a higher number of particles taken up per cell in tumor-bearing mice (Figure 6A,C; bottom). The M2-like macrophages in all three organs were more active in particle uptake when a tumor was present, as the MFI increased significantly between the naïve and A549 lung mice. Overall, we observed that all macrophages were more efficient at particle sequestration in the tumor-bearing animals, where the M2-like macrophage population was up-regulated and showed increased recognition of particles.

Discussion

Tumor presence is known to alter the status of the immune system from Th1 to Th2,[13,17] but only recently have studies emerged on the effect of this shift on particle behavior. Previous work in healthy mice discovered a particle clearance difference in strains with genetically biased immune function.[18] Increased clearance was observed in Th2-biased mice compared to Th1-biased strains. The current study showed a comparable trend in particle behavior based on tumor presence. Our results show that a normally Th1-biased mouse strain (C57BL/6 background) can exhibit particle clearance behavior more similar to Th2-biased mouse strain following the induction of a tumor. This study highlights the impact of shifting immune status with disease progression and how this in turn can dramatically impact nanoparticle behavior.

Increased particle clearance was observed in both IVM and ICP-MS studies between nontumor and tumor bearing mice. The quantitative analysis by ICP-MS reported herein revealed the tumor-induced immune shift was the most prominent in the liver, where early rapid accumulation was evident in mice with tumors compared to controls. This large difference in the initial level of PRINT hydrogel nanoparticles in the liver and plasma could be explained by a shift in macrophage activity, with an increase in M2-like macrophages. The liver receives nearly two-thirds of the blood volume per minute and contains over 75% of the total tissue macrophage population.[32,33] An increase in the particle affinity of macrophages in the liver would have a dramatic effect on particle clearance, which could be induced through the presence of a tumor. The tumor microenvironment displays a local Th2-bias and, in some cases, can cause a systemic shift as well.[13,34] Several studies have shown that the presence of a tumor activates the M2-like macrophage subset population, which corroborates our results in Figure 5.[17,31,35] M2-polarized macrophages have increased phagocytic and scavenging ability, which resulted in more efficient particle sequestration.[36] The increased recognition of PRINT particles by macrophages, especially by M2-like macrophages, can account for the decrease in particle circulation in the presence of a tumor; however, the increase in both subsets suggests other factors may also be responsible for the difference in clearance. For instance, in a study by Caron *et al*., increased phagocytic

activity of circulating monocytes was correlated with increased nanoparticle clearance in humans.[37] This trend was also observed in our results of Figure 4A. Another study investigated the effect of certain chemokines on the circulation and accumulation of PEGylated liposomal doxorubicin (Doxil) in both naïve and tumor-bearing animals, with results similar to those reported here.[38] These studies provide further evidence that multiple factors can be responsible for a shift in particle behavior.

The changes in immune status and the activation of M2-like macrophages led us to hypothesize that the tumor cells or microenvironment was secreting a factor capable of skewing phagocytic capacity. The ability to mimic the difference in particle recognition in *ex vivo* macrophages showed a serum-resident factor was at least partially responsible for the increase in liver and spleen sequestration upon tumor presence. Literature evidence suggests that tumor cells secrete factors that can directly affect and change macrophage activity. Previous studies have shown the ability of cancer cells to polarize macrophages, utilizing cytokine analysis, immunohistochemistry, and gene amplification to characterize the effects of coculturing macrophages with cancer cells.[39–41] In a study by Muller-Quernheim *et al.*, both the coculture of tumor cells with macrophages and the treatment of macrophages with media taken from tumor cell cultures resulted in an increased activity for both M1 and M2-like macrophages, with a slight skewing toward a M2-like phenotype.[42] Furthermore, this study used A549 cells, the same line investigated in the work presented here. Similar results would be expected in the other two tumor models, although potentially to a lesser degree due to the syngeneic nature of the cancer cells. In the A549 model investigated, the initial bias toward a M1 macrophage phenotype in the liver and spleen is supported by the genetic predisposition of the C57BL/6 background nude mice used in this study toward a Th1-bias immune system.[43] More in-depth studies to identify the specific factor(s) responsible for the shift in immune cell activity are needed and currently underway. The tumor microenvironment is heterogeneous, and identifying a specific factor among the myriad of cytokines, chemokines, growth factors, cell signaling molecules, and countless other moieties presents unique challenges. However, recent work has provided several areas to focus on in the search, such as galectins, MHC protein homologues, CTLA-4, PD-1, and a variety of anti-inflammatory interleukins (*i.e.*, IL-4, IL-13).[44]

The results presented here demonstrate that the presence of a tumor can alter a local and global immune system, which in turn has dramatic effects on nanoparticle circulation and potential efficacy. Interestingly, we observed a decrease in particle circulation between tumor-bearing and nontumor-bearing mice regardless of tumor type and location. However, there were slight differences observed between the various models chosen; the human lung xenograft (A549) showed the largest increase in particle clearance, with the mouse lung allograft (344SQ) and mouse melanoma allograft (LKB498) in the ear also showing an increase compared to naive controls. All of these models were induced in female Foxn1nu (athymic nude, C57BL/6J background) mice, yet a considerable difference was still apparent based on tumor presence. We hypothesize that a similar shift from a Th1- to Th2-biased immune status was responsible for the increased clearance in each of these tumor models. Understanding the role of these changing phenotypes on nanoparticle interaction offers an opportunity for increasing nanoparticle efficacy; mitigation or reversal of the systemic shift

could be achieved by incorporating a scavenging moiety onto the particle to sequester the circulating factor and reduce immune evasion by the tumor. Alternative approaches using immunotherapy could harness the macrophage's affinity for particles and co-opt a change in status by delivering a stimulant to the macrophage, reversing the polarization to promote an antitumor M1 phenotype.

Conclusion

Our work highlights the important interplay between immune status, disease progression, and nanoparticle properties. To evaluate nanoparticle efficacy, an animal model must be chosen which has an immune status similar to the actual disease. For a given tumor cell line, mouse strain, and tumor location, differences in secreted factors and resultant changes in cellular function will affect particle clearance properties. Thus, prior characterization of the model itself will be essential to evaluating the preclinical success of a given nanoparticle therapeutic. Furthermore, a given immune status may be predictive of nanoparticle success. This has important clinical ramifications. Further evaluation of a patient's immune function following similar evaluations to those presented here may be important predictors of nanoparticle success in a clinical setting.

Methods

Materials

Commercially available polyethylene glycol diacrylate (PEG_{700}-DA) (M_n = 700 Da), 2-aminoethyl methacrylate hydrochloride (AEM), diphenyl(2,4,6-trimethylbenzoyl)-phosphine oxide (TPO), poly(vinyl alcohol) (PVOH, M_n = 2000 Da), succinic anhydride, cis-diaminedichloroplatinum(II) (CDDP), and sucrose were purchased from Sigma-Aldrich. PTFE syringe filters (13 mm membrane, 0.220 μm pore size), Dylight 488 maleimide, Dylight 650 maleimide, dimethylformamide (DMF), triethylamine (TEA), pyridine, sterile water, borate buffer (pH 8.6), methanol, trace-metal grade concentrated nitric acid (HNO_3), Corning Matrigel Membrane Matrix (LDEV-free), EDTA-treated collection tubes, cell strainers, 4% paraformaldehyde (PFA), and ACK buffer were obtained from Fisher Scientific. Methoxy PEG (5k)-succinimidyl carboxy methyl ester (mPEG5k-SCM) was purchased from Creative PEGWorks. Tetraethylene glycol monoacrylate (HP_4A) was synthesized in-house as previously described.[45] Conventional filters (2 μm) were purchased from Agilent, and poly(vinyl alcohol) (M_w 2000) (PVOH) was purchased from Acros Organics. PRINT molds (80 nm × 320 nm) were obtained from Liquidia Technologies (Morrisville, NC). Polyethylene terephthalate (PET) was purchased in 1000-foot rolls from 3M. Cisplatin was acquired from the University of North Carolina Pharmacy. Water, where used, was sterile-grade and 0.2-μm filtered. A549-luc, LKB498, and L929 cells were purchased from American Type Culture Collection. 344SQ cells were a gift from The University of Texas M.D. Anderson Cancer Center (Jon Kurie Lab). All cells were maintained per vendor specifications. Fetal bovine serum was purchased from Atlanta Biologicals. Hank's Balanced Salt Solution (HBSS), RPMI 1640 Medium, and Dulbecco's Modified Eagle Medium (DMEM) were purchased from Gibco. All commercially available materials were used as received. Anti-mouse antibodies (CD45-Pac Blue, CD11c-PE,

CD206-PE, CD11b-Brilliant Violet 605, CD19-PE-Cy7, F4/80-APC, Ly6G/C-PE-Cy5) were purchased from BioLegend, Inc. Lymphoprep, DNase, and collagenase were purchased from STEMCELL Technologies, Inc. AbC Anti-Mouse Bead Kit and anti-CD16/32 (Fc-block) were purchased from Invitrogen. FACS buffer was prepared as HBSS plus 2% FBS.

Particle Fabrication and Characterization

PRINT 80 nm × 320 nm hydrogel particles were fabricated and functionalized with a PEG mushroom surface as described in ref 22, and a more detailed description can be found in Supporting Information. Particles were then succinylated by reaction with an excess of pyridine and succinic anhydride (100× molar excess with respect to amine groups). The reaction was carried out in a sonicator bath (Branson Ultrasonic Cleaner 1.4 A, 160 W) for 30 min. Following succinylation, the particles were washed by centrifugation one time in DMF, followed by a borate buffer wash to neutralize any succinic acid side product, and then three washes with sterile water.

Cisplatin complexation was achieved by incubating the particles in a solution of CDDP (2× molar excess with respect to carboxyl groups) in water at room temperature for >24 h under constant agitation (Eppendorf, 1400 rpm). After incubation in the complexation solution, particles were washed with sterile water by centrifugation and resuspended in 9.25 wt % sucrose (aq) at the appropriate dose concentration. Aliquots were flash frozen in liquid nitrogen and stored at −20 °C until needed. Dylight 650 and 488 were used for the intravital and flow cytometry studies, respectively. PRINT-cisplatin was used without a fluorophore for the inductively coupled-mass spectroscopy (ICP-MS) studies.

Particle concentrations were determined by thermogravimetric analysis (TGA) using a TAInstruments Q5000 analyzer. Particle size and zeta potential were verified by dynamic light scattering (DLS) on a Zetasizer Nano ZS (Malvern Instruments, Ltd.) at 37 °C. Cisplatin loading was assessed using an Agilent 1200 series high-performance liquid chromatography system with an ultraviolet detector. The mobile phase consisted of 90% 0.9-wt % NaCl (aq) and 10% methanol, by volume. A 5 min isocratic elution protocol was used with a ZORBAX Eclipse Plus C18 column (Agilent Technologies). The product was eluted at a flow rate of 1 mL/min and monitored at a wavelength of 210 nm. Drug loading was determined by analysis of the complexation solution pre- and postincubation. The net difference in cisplatin concentration was calculated as weight percent in the particle.

Animals

All experiments involving mice were performed in accordance with the National Research Council's Guide to Care and Use of Laboratory Animals (1996), under an animal use protocol approved by the University of North Carolina Animal Care and Use Committee. All studies used female *Foxn1*^{nu} (athymic nude, C57BL/6J background) mice (5 weeks old, 17–27 g, Jackson Laboratory). For the tumor-bearing mice, two orthotopic non-small cell lung models (A549-luc and 344SQ) and an orthotopic melanoma (LKB498) model were used. Cell cultures were prepared and maintained per vendor specifications. The orthotopic lung surgery was performed by injection of a 40 μL suspension of either A549 cells (5×10^6 cells per mouse) or 344SQ cells (5000 cells per mouse) in a 50:50 Matrigel:PBS blend into

the lung *via* intrathoracic inoculations, as per published protocol.[46] Tumors were grown to 100–200 mm^3 total cumulative volume (caliper measurement for LKB498, orthotopic A549luc and 344SQ verified by measurement following thoracotomy). Sham mice underwent the surgical procedure and received the Matrigel:PBS suspension injection without cells. For the orthotopic ear allograft, a single spheroid of approximately 4000 LKB498 cells was injected intradermally as previously described.[47] All nanoparticles were dosed in 9.25 wt % sucrose to maintain isotonicity upon intravenous administration.

Ex Vivo Macrophage Association

Primary macrophages were isolated from the bone marrow of nude mice per established protocol.[48] Briefly, mice were euthanized, and the femur and tibia bones were resected. Bone marrow cells were collected by flushing the marrow cavity with HBSS + 2% FBS. Cells were filtered and plated with L929-conditioned medium (containing GM-CSF) to promote differentiation and growth of macrophages from precursor cells within the marrow. Cells were incubated with or without serum collected from naïve and tumor-bearing mice. After 24 h, the serum-spiked media was replaced with fresh, nonspiked media, and fluorescent PRINT hydrogel nanoparticles were dosed at 1 mg/mL for 3 h. Cells were then collected and fixed with 4% PFA for analysis by flow cytometry.

Intravital Microscopy Study

Particles containing Dylight 650 were injected and analyzed by intravital microscopy as described in ref 22. Briefly, experiments were performed using an IV 100 laser scanning microscope (Olympus). Mice (n = 5) were anesthetized with isofluorane, a tail vein catheter was applied, and animals were placed on a 37 °C heated stage in the prone position and kept under anesthesia. The ear was immobilized to an aluminum block with double-sided tape, and vasculature was visualized with a 488 nm laser; the nontumor-bearing ear was used in studies with the LKB498 mice. Mice were then dosed with a bolus injection of Dylight 650-labeled nanoparticles. Fluorescence was measured using a 633 nm laser, and imaging scans were captured every 5 s for 2 h. For circulation analysis, the image files from each scan were exported to ImageJ. Following literature procedures, the images were stacked in groups of four, and fluorescent signal in each stack was analyzed in the region of interest (ROI).[23,49] Background corrections were obtained using the initial fluorescence in the ROI before injection. All instrument settings were kept constant for the duration of the study. Particles were dosed at 18.75 mg per kg of body weight.

ICP-MS study

Quantification of cisplatin and PRINT-cisplatin was performed using ICP-MS. Cisplatin and PRINT particles were dosed with a bolus intravenous injection at an equivalent of 3 mg per kg drug, which corresponded to a particle dose of 18.75 mg/kg. Liver, spleen, lung, and kidney were harvested and flash-frozen in liquid nitrogen at 0.083, 0.5, 1, 6, and 24 h postinjection. Tumor accumulation was not determined due to tumor cell heterogeneity with the lung cells within the organ in the orthotopic A549 model. Four mice per arm were examined at each time point. Blood was collected in EDTA by cardiac puncture at the same time points and centrifuged (300*g*, 5 min, 4 °C) to isolate plasma from the cell fraction.

Tissue sample preparation was performed as previously described.[6] Briefly, tissue and plasma samples were digested in concentrated HNO_3 spiked with 200 ng/mL Iridium (Ir; analytical internal standard, Inorganic Ventures) for 60–90 min at 90 °C. Deionized water was added to bring sample to volume and HNO_3 concentration of 3.5%, and the samples were stored at 4 °C until platinum (Pt) analysis was completed. ICP-MS analysis (Agilent 7500cx) was performed and validated as previously described.[6,26] Pharmacokinetic analysis of the measured plasma concentrations was performed using PKSolver.[50] Data was fit to either a one- or two-compartment model, and the Akaike information criterion (AIC) was used to compare goodness of fit for each nanoparticle type.[51]

Tissue Preparation for Immune Cell Analysis

Once the A549 lung tumors had grown to sufficient size, both tumor-bearing and naïve mice were injected with a bolus intravenous suspension of PRINT hydrogel particles containing Dylight 488 at 18.75 mg/kg (n = 5). Additional tumor-bearing and naïve mice were given a bolus intravenous saline injection for use as controls (n = 3). Two hours postinjections, mice were euthanized and blood was collected *via* cardiac puncture and stored on ice in EDTA-treated collection tubes. The thoracic cavity was opened to visualize the heart. The right atrium was nicked, and organs were perfused with a HBSS flush *via* the left ventricle. The lung, spleen, and liver were resected and stored on ice. Spleens were mechanically forced through a cell strainer to dissociate tissue into FACS buffer. Lungs and livers were incubated at 37 °C, 5% CO_2 in digestion media (HBSS + 2% FBS + 0.02 mg/mL DNase and 1 mg/mL collagenase) until dissociated. ACK buffer was used to lyse red blood cells in blood, lung, and spleen, and samples were subsequently passed through a cell strainer to remove aggregates and excess debris. Immune cells were isolated from livers using Lymphoprep, per manufacturer's guidelines. This resulted in single cell suspensions of blood, lung, spleen, and liver tissues. Samples were blocked with anti-CD16/32 (Fc-block) and stained with a panel of antibodies. Lung, spleen, and liver samples were split into two equal aliquots. One aliquot, along with blood samples, received Panel A: CD45-Pac Blue, CD11b-Brilliant Violet 605, CD11c-PE, Ly6G-PE-Cy5, F4/80-APC, and CD19-PE-Cy7. The remaining lung, spleen, and liver aliquots received Panel B: CD45-Pac Blue, CD11b-Brilliant Violet 605, F4/80-APC, and CD206-PE. All samples were fixed with 4% PFA and stored for analysis by flow cytometry.

Flow Cytometry

Samples of single cell suspensions from blood, lung, spleen, and liver of naïve and tumor-bearing mice were analyzed with an LSRII (BD Biosciences) flow cytometer. AbC Anti-Mouse Beads were labeled with each of the fluorophore-antibody and used to compensate for each fluorescence channel. Fluorescence minus one (FMO) samples were prepared from untreated cell suspensions for delineation of positive and negative antibody expression on cells. Representative sample gating for Panel A and Panel B is depicted in Supporting Information Figures 3 and 4, respectively. Samples from the *ex vivo* macrophage association study were analyzed as described, and utilized only forward scatter, side scatter, and the Dylight 488 fluorescence channel and did not require compensation or FMO samples. FlowJo software (Tree Star) was used to analyze data per literature precedence and guidance.[18,52]

Statistics

Analysis of Variance (ANOVA) was performed in GraphPad Prism using the Bonferroni post-test. All error bars represent of standard error mean.

Supplementary Material

Refer to Web version on PubMed Central for supplementary material.

Acknowledgments

The authors would like to thank Charlene Santos and the UNC Animal Studies Core for their help with the murine experiments. We also thank Peter Cable for his expertise with ICP-MS analysis, Sara O'Neal for help with pharmacokinetic data collection and analysis, and Dr. Ashish Pandya for the synthesis of HP_4A. This work was supported by Liquidia Technologies, the Carolina Center for Cancer Nanotechnology Excellence U54CA151652 and U54CA198999 (to J.P.-Y.T. and J.M.D.), NIH Pioneer Award 1DP1OD006432 (to J.M.D.), NIH Grant U19AI109784 (to J.P.-Y.T. and J.M.D.), and Defense Threat Reduction Agency (DTRA) Award HDTRA1-13-1-0045 (to J.M.D.).

References

1. Wang AZ, Langer R, Farokhzad OC. Nanoparticle Delivery of Cancer Drugs. Annu Rev Med. 2012; 63:185–198. [PubMed: 21888516]
2. Fidler IJ. Rationale and Methods For the Use of Nude Mice to Study the Biology and Therapy of Human Cancer Metastasis. Cancer Metastasis Rev. 1986; 5:29–49. [PubMed: 2942306]
3. Marusyk A, Almendro V, Polyak K. Intra-Tumour Heterogeneity: A Looking Glass For Cancer? Nat Rev Cancer. 2012; 12:323–334. [PubMed: 22513401]
4. Balkwill FR, Capasso M, Hagemann T. The Tumor Microenvironment at a Glance. J Cell Sci. 2012; 125:5591–5596. [PubMed: 23420197]
5. Whiteside TL. The Tumor Microenvironment and Its Role in Promoting Tumor Growth. Oncogene. 2008; 27:5904–5912. [PubMed: 18836471]
6. Combest AJ, Roberts PJ, Dillon PM, Sandison K, Hanna SK, Ross C, Habibi S, Zamboni B, Muller M, Brunner M, et al. Genetically Engineered Cancer Models, But Not Xenografts, Faithfully Predict Anticancer Drug Exposure in Melanoma Tumors. Oncologist. 2012; 17:1303–1316. [PubMed: 22993143]
7. Richmond A, Su Y. Mouse Xenograft Models vs GEM Models For Human Cancer Therapeutics. Dis Models & Mech. 2008; 1:78–82.
8. Nel AE, Madler L, Velegol D, Xia T, Hoek EMV, Somasundaran P, Klaessig F, Castranova V, Thompson M. Understanding Biophysicochemical Interactions at the Nano-BioInterface. Nat Mater. 2009; 8:543–557. [PubMed: 19525947]
9. Albanese A, Tang PS, Chan WCW. The Effect of Nanoparticle Size, Shape, and Surface Chemistry on Biological Systems. Annu Rev Biomed Eng. 2012; 14:1–16. [PubMed: 22524388]
10. Owens DE III, Peppas NA. Opsonization, Biodistribution, and Pharmacokinetics of Polymeric Nanoparticles. Int J Pharm. 2006; 307:93–102. [PubMed: 16303268]
11. Sun X, Rossin R, Turner JL, Becker ML, Joralemon MJ, Welch MJ, Wooley KL. An Assessment of the Effects of Shell Cross-Linked Nanoparticle Size, Core Composition, and Surface PEGylation on *In Vivo* Biodistribution. Biomacromolecules. 2005; 6:2541–2554. [PubMed: 16153091]
12. Kiessling R, Wasserman K, Horiguchi S, Kono K, Sjöberg J, Pisa P, Petersson M. Tumor-Induced Immune Dysfunction. Cancer Immunol Immunother. 1999; 48:353–362. [PubMed: 10501847]
13. Shurin MR, Lu L, Kalinski P, Stewart-Akers AM, Lotze MT. Th1/Th2 Balance in Cancer, Transplantation and Pregnancy. Springer Semin Immunopathol. 1999; 21:339–359. [PubMed: 10666777]

14. Bronte V, Serafini P, Apolloni E, Zanovello P. Tumor-Induced Immune Dysfunctions Caused by Myeloid Suppressor Cells. J Immunother. 2001; 24:431–446. [PubMed: 11759067]
15. Kusmartsev S, Gabrilovich DI. Immature Myeloid Cells and Cancer-Associated Immune Suppression. Cancer Immunol Immunother. 2002; 51:293–298. [PubMed: 12111117]
16. Serafini P, De Santo C, Marigo I, Cingarlini S, Dolcetti L, Gallina G, Zanovello P, Bronte V. Derangement of Immune Responses by Myeloid Suppressor Cells. Cancer Immunol Immunother. 2004; 53:64–72. [PubMed: 14593498]
17. Sica A, Bronte V. Altered Macrophage Differentiation and Immune Dysfunction in Tumor Development. J Clin Invest. 2007; 117:1155–1166. [PubMed: 17476345]
18. Jones SW, Roberts RA, Robbins GR, Perry JL, Kai MP, Chen K, Bo T, Napier ME, Ting JPY, DeSimone JM, et al. Nanoparticle Clearance is Governed by Th1/Th2 Immunity and Strain Background. J Clin Invest. 2013; 123:3061–3073. [PubMed: 23778144]
19. Euliss LE, DuPont JA, Gratton S, DeSimone J. Imparting Size, Shape, and Composition Control of Materials for Nanomedicine. Chem Soc Rev. 2006; 35:1095–1104. [PubMed: 17057838]
20. Rolland JP, Maynor BW, Euliss LE, Exner AE, Denison GM, DeSimone JM. Direct Fabrication and Harvesting of Monodisperse, Shape-Specific Nanobiomaterials. J Am Chem Soc. 2005; 127:10096–10100. [PubMed: 16011375]
21. Kersey FR, Merkel TJ, Perry JL, Napier ME, Desimone JM. Effect of Aspect Ratio and Deformability on Nanoparticle Extravasation Through Nanopores. Langmuir. 2012; 28:8773–8781. [PubMed: 22612428]
22. Perry JL, Reuter KG, Kai MP, Herlihy KP, Jones SW, Luft JC, Napier M, Bear JE, DeSimone JM. PEGylated PRINT Nanoparticles: The Impact of PEG Density on Protein Binding, Macrophage Association, Biodistribution, and Pharmacokinetics. Nano Lett. 2012; 12:5304–5310. [PubMed: 22920324]
23. Merkel TJ, Jones SW, Herlihy KP, Kersey FR, Shields AR, Napier M, Luft JC, Wu H, Zamboni WC, Wang AZ, et al. Using Mechanobiological Mimicry of Red Blood Cells to Extend Circulation Times of Hydrogel Microparticles. Proc Natl Acad Sci U S A. 2011; 108:586–591. [PubMed: 21220299]
24. Hughes EL, Gavins FNE. Troubleshooting methods: Using Intravital Microscopy in Drug Research. J Pharmacol Toxicol Methods. 2010; 61:102–112. [PubMed: 20097299]
25. Hu W, Pasare C. Location, Location, Location: Tissue-Specific Regulation of Immune Responses. J Leukocyte Biol. 2013; 94:409–421. [PubMed: 23825388]
26. Morrison JG, White P, McDougall S, Firth JW, Woolfrey SG, Graham MA, Greenslade D. Validation of a Highly Sensitive ICP-MS Method for the Determination of Platinum in Biofluids: Application to Clinical Pharmacokinetic Studies With Oxaliplatin. J Pharm Biomed Anal. 2000; 24:1–10. [PubMed: 11108533]
27. Kai MP, Keeler AW, Perry JL, Reuter KG, Luft JC, O'Neal SK, Zamboni WC, DeSimone JM. Evaluation of Drug Loading, Pharmacokinetic Behavior, and Toxicity of a Cisplatin-Containing Hydrogel Nanoparticle. J Controlled Release. 2015; 204:70–7.
28. Kwon M, Berns A. Mouse Models for Lung Cancer. Mol Oncol. 2013; 7:165–177. [PubMed: 23481268]
29. Mantovani A, Locati M. Tumor-Associated Macrophages as a Paradigm of Macrophage Plasticity, Diversity, and Polarization: Lessons and Open Questions. Arterioscler, Thromb, Vasc Biol. 2013; 33:1478–1483. [PubMed: 23766387]
30. Mantovani A, Sozzani S, Locati M, Allavena P, Sica A. Macrophage Polarization: Tumor-Associated Macrophages as a Paradigm for Polarized M2Mononuclear Phagocytes. Trends Immunol. 2002; 23:549–555. [PubMed: 12401408]
31. Gabrilovich DI, Ostrand-Rosenberg S, Bronte V. Coordinated Regulation of Myeloid Cells by Tumours. Nat Rev Immunol. 2012; 12:253–268. [PubMed: 22437938]
32. Jenne CN, Kubes P. Immune Surveillance by the Liver. Nat Immunol. 2013; 14:996–1006. [PubMed: 24048121]
33. Sheth K, Bankey P. The Liver as an Immune Organ. Curr Opin Crit Care. 2001; 7:99–104. [PubMed: 11373518]
34. Finn OJ. Cancer Immunology. N Engl J Med. 2008; 358:2704–2715. [PubMed: 18565863]

35. Van Ginderachter J, Meerschaut S, Liu Y, Brys L, De Groeve K, Hassanzadeh Ghassabeh G, Raes G, De Baetselier P. Peroxisome Proliferator-Activated Receptor Gamma (PPARgamma) Ligands Reverse CTL Suppression by Alternatively Activated (M2) Macrophages in Cancer. Blood. 2006; 108:525–535. [PubMed: 16527895]
36. Biswas SK, Mantovani A. Macrophage Plasticity and Interaction With Lymphocyte Subsets: Cancer as a Paradigm. Nat Immunol. 2010; 11:889–896. [PubMed: 20856220]
37. Caron WP, Lay JC, Fong AM, La-Beck NM, Kumar P, Newman SE, Zhou H, Monaco JH, Clarke-Pearson DL, Brewster WR, et al. Translational Studies of Phenotypic Probes for the Mononuclear Phagocyte System and Liposomal Pharmacology. J Pharmacol Exp Ther. 2013; 347:599–606. [PubMed: 24042160]
38. Song G, Tarrant TK, White TF, Barrow DA, Santos CM, Timoshchenko RG, Hanna SK, Ramanathan RK, Lee CR, Bae-Jump VL, et al. Roles of Chemokines CCL2 and CCL5 in the Pharmacokinetics of PEGylated Liposomal Doxorubicin *in vivo* and in Patients With Recurrent Epithelial Ovarian Cancer. Nanomedicine. 2015; 11:1797–1807. [PubMed: 26093057]
39. Yuan Z, Mehta HJ, Mohammed K, Nasreen N, Roman R, Brantly M, Sadikot RT. TREM-1 is Induced in Tumor Associated Macrophages by Cyclo-oxygenase Pathway in Human Non-Small Cell Lung Cancer. PLoS One. 2014; 9:e94241. [PubMed: 24842612]
40. Cho HJ, Jung JI, Lim DY, Kwon GT, Her S, Park JH, Park JH. Bone Marrow-Derived, Alternatively Activated Macrophages Enhance Solid Tumor Growth and Lung Metastasis of Mammary Carcinoma Cells in a Balb/C Mouse Orthotopic Model. Breast Cancer Res. 2012; 14:R81. [PubMed: 22616919]
41. Han W, Joo M, Everhart MB, Christman JW, Yull FE, Blackwell TS. Myeloid Cells Control Termination of Lung Inflammation Through the NF-kappaB Pathway. Am J Physiol Lung Cell Mol Physiol. 2009; 296:L320–327. [PubMed: 19098124]
42. Muller-Quernheim UC, Potthast L, Muller-Quernheim J, Zissel G. Tumor-Cell Co-Culture Induced Alternative Activation of Macrophages is Modulated by Interferons *In Vitro*. J Interferon Cytokine Res. 2012; 32:169–177. [PubMed: 22280057]
43. Petkova SB, Yuan R, Tsaih S, Schott W, Roopenian DC, Paigen B. Genetic Influence on Immune Phenotype Revealed Strain-Specific Variations in Peripheral Blood Lineages. Physiol Genomics. 2008; 34:304–314. [PubMed: 18544662]
44. Burkholder B, Huang RY, Burgess R, Luo S, Jones VS, Zhange W, Lv ZQ, Gao CY, Wang BL, Zhang YM, et al. Tumor-Induced Perturbations of Cytokines and Immune Cell Networks. Biochim Biophys Acta, Rev Cancer. 2014; 1845:182–201.
45. Guzmán J, Iglesias MT, Riande E, Compañ V, Andrio A. Synthesis and Polymerization of Acrylic Monomers With Hydrophilic Long Side Groups. Oxygen Transport Through Water Swollen Membranes Prepared From These Polymers. Polymer. 1997; 38:5227–5232.
46. Peng L, Feng L, Yuan H, Benhabbour SR, Mumper RJ. Development of a Novel Orthotopic Non-Small Cell Lung Cancer Model and Therapeutic Benefit of 2′-(2-Bromohexadecanoyl)-Docetaxel Conjugate Nanoparticles. Nanomedicine. 2014; 10:1497–1506. [PubMed: 24709328]
47. Rozenberg GI, Monahan KB, Torrice C, Bear JE, Sharpless NE. Metastasis in an Orthotopic Murine Model of Melanoma is Independent of RAS/RAF Mutation. Melanoma Res. 2010; 20:361–371. [PubMed: 20679910]
48. Weischenfeldt J, Porse B. Bone Marrow-Derived Macrophages (BMM): Isolation and Applications. Cold Spring Harb Protoc. 2008; 3:1–6.
49. Tong L, He W, Zhang Y, Zheng W, Cheng JX. Visualizing Systemic Clearance and Cellular Level Biodistribution of Gold Nanorods by Intrinsic Two-Photon Luminescence. Langmuir. 2009; 25:12454–12459. [PubMed: 19856987]
50. Zhang Y, Huo M, Zhou J, Xie S. PKSolver: An Add-in Program for Pharmacokinetic and Pharmacodynamic Data Analysis in Microsoft Excel. Comput Methods Programs Biomed. 2010; 99:306–314. [PubMed: 20176408]
51. Akaike H. A New Look at the Statistical Model Identification. IEEE Trans Autom Control. 1974; 19:716–723.
52. Herzenberg L, Tung J, Moore W, Herzenberg L, Parks DR. Interpreting Flow Cytometry Data: A Guide for the Perplexed. Nat Immunol. 2006; 7:681–685. [PubMed: 16785881]

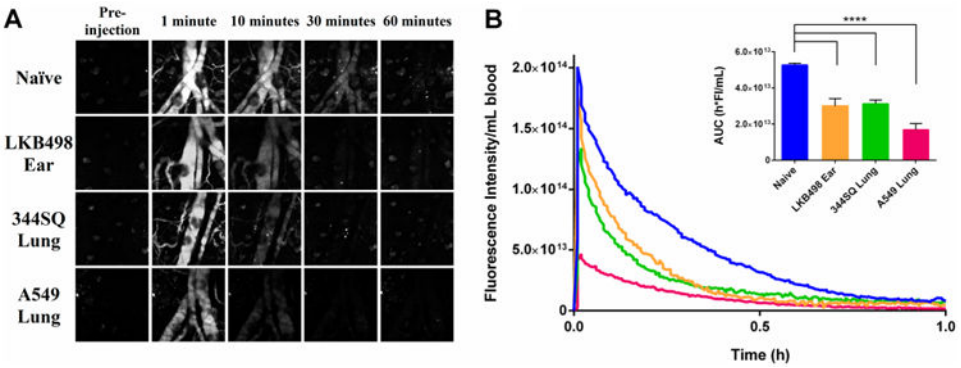

Figure 1.

Circulation of intravenously injected PRINT hydrogels is reduced in tumor-bearing mice. (A) Still images from intravital microscopy in naïve and tumor-bearing mice depict lower initial fluorescence and faster clearance in tumor-bearing mice compared to naïve mice (scale-bar = 50 μm). (B) Particle fluorescence in blood over time and exposure (inset) expressed as area-under-the-curve reveals a tumor-induced pharmacokinetic modulation. (****$p < 0.0001$; one-way ANOVA).

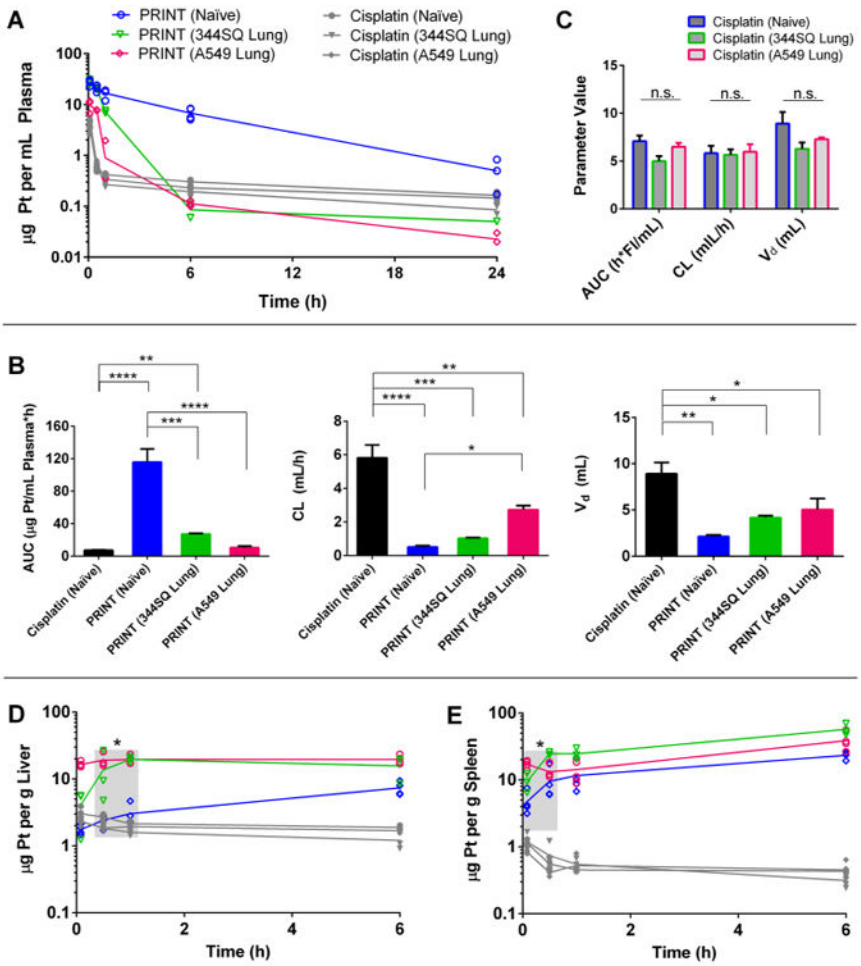

Figure 2.

Tumor presence alters nanoparticle circulation and accumulation in organs with salient immune cell activity. The plasma profile (A) and pharmacokinetic parameters (B) of particles were significantly altered by the presence of a tumor, including exposure (AUC), clearance rate from circulation (CL), and volume of distribution (V_d). The behavior of free cisplatin, however, remained unaffected (C). Additionally, there was a significant increase in initial sequestration of particles in both liver (D) and spleen (E) in tumor-bearing mice compared to naïve mice. Measured as platinum (Pt) content *via* inductively coupled plasma mass spectroscopy (*$p < 0.05$, **$p < 0.01$, ***$p < 0.001$, ****$p < 0.0001$; one-way ANOVA).

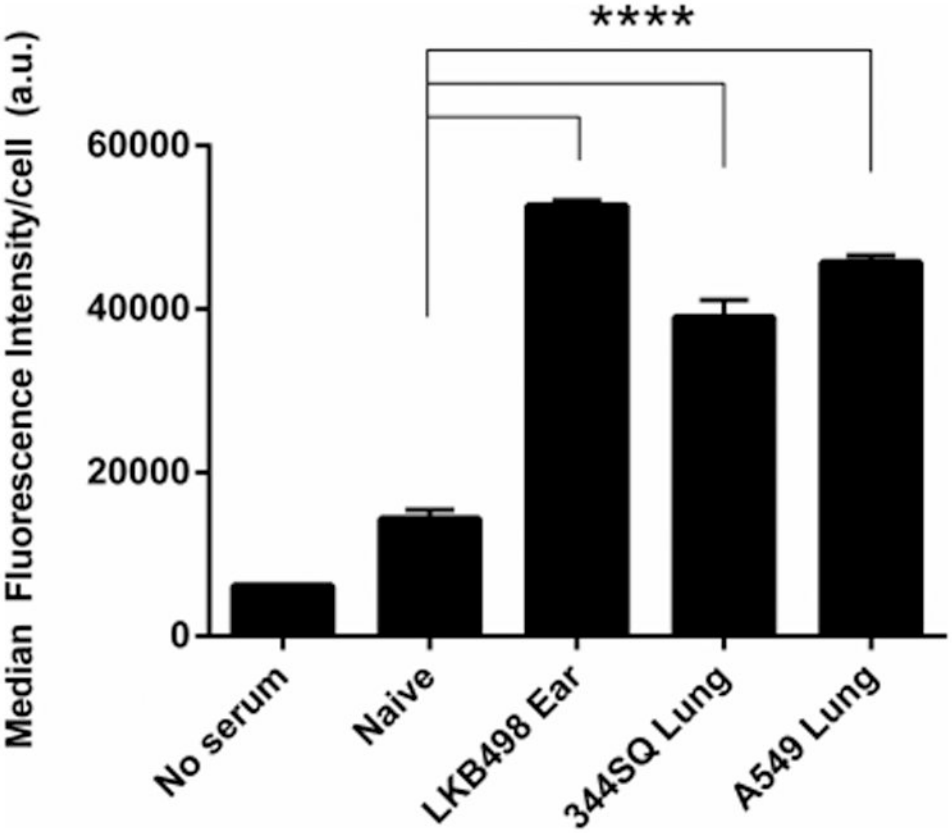

Figure 3.

Serum collected from tumor-bearing mice induced an increase in *ex vivo* macrophage activity compared to serum collected from naïve mice. PRINT hydrogel nanoparticle association with *ex vivo* macrophages incubated with serum from naïve and tumor-bearing mice (****$p < 0.0001$; one-way ANOVA).

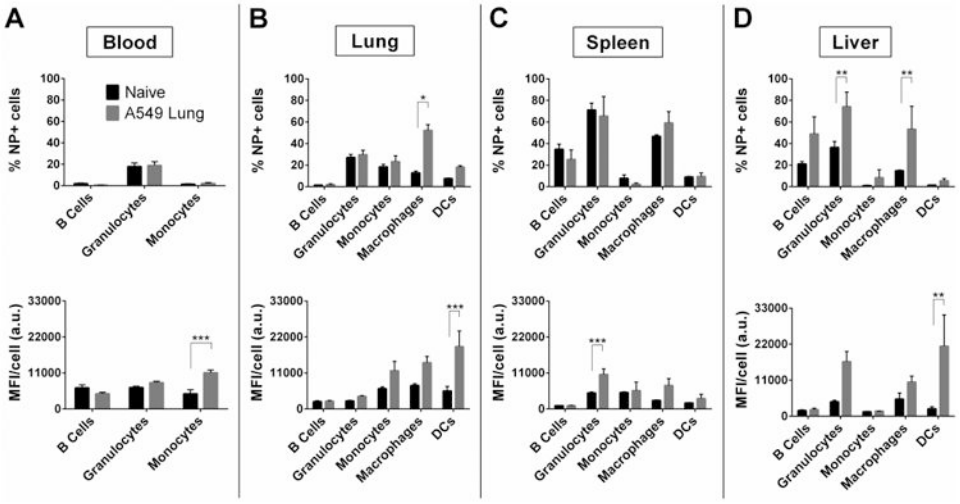

Figure 4.

Tumor presence alters immune cell interactions with particles. Immune cell distribution of PRINT hydrogel nanoparticles in blood (A), lung (B), spleen (C), and liver (D). Significant increases in association and MFI were seen for several populations, including macrophages and dendritic cells in the lung and liver. MFI = median fluorescence intensity (*$p < 0.05$, **$p < 0.01$, ***$p < 0.001$; two-way ANOVA).

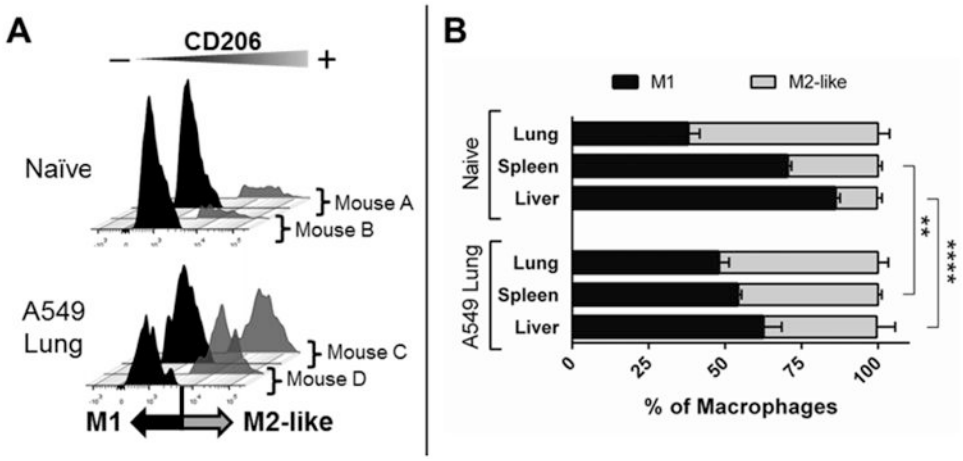

Figure 5.

Presence of A549 tumors skewed macrophage populations from M1 to M2-like. Representative flow cytometry histograms (A) of CD206 expression in macrophages of the liver show an increase in M2-like phenotype in tumor-bearing mice. A significant increase in the population of liver and spleen M2-like macrophages (B) was observed in tumor-bearing mice compared to naïve mice (**$p < 0.01$, ****$p < 0.0001$; two-way ANOVA).

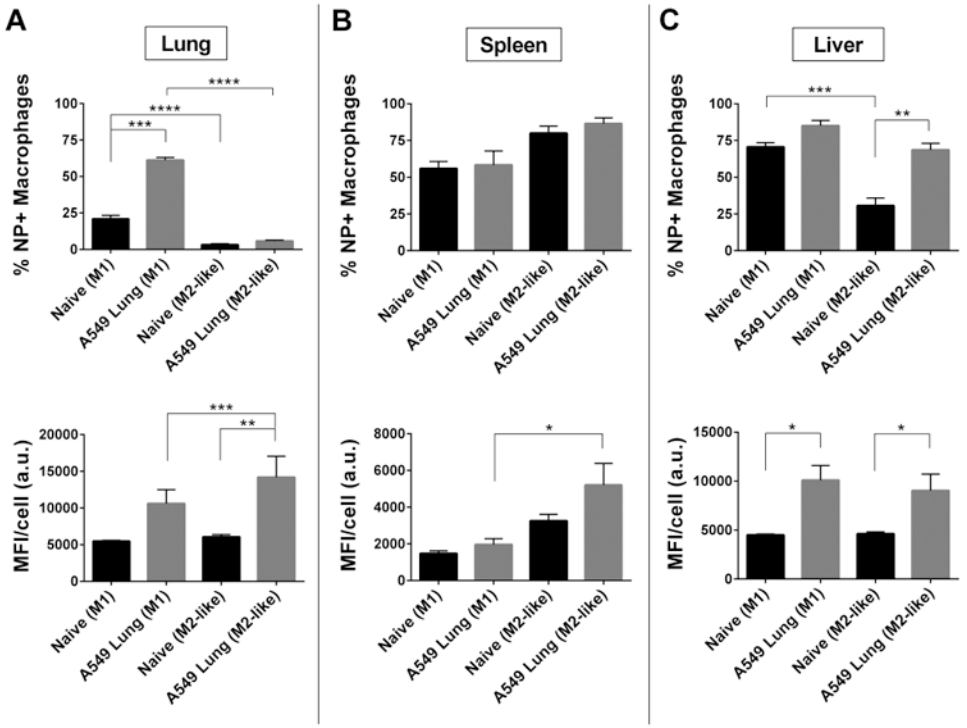

Figure 6.

M1 and M2-like macrophages have higher affinity for nanoparticles in tumor-bearing mice. Macrophage subset association of PRINT hydrogel nanoparticles by flow cytometry in lung (A), spleen (B), and liver (C) of tumor-bearing and naïve mice. Differences in particle association and MFI were revealed: significant increases in the same macrophage subset between naïve and tumor-bearing mice, and also between different macrophage subsets within the same mouse model. MFI = median fluorescence intensity (*$p < 0.05$, **$p < 0.01$, ***$p < 0.001$, ****$p < 0.0001$; two-way ANOVA).